Toxicogenomics of nanoparticulate delivery of etoposide: potential impact on nanotechnology in retinoblastoma therapy

Moutushy Mitra · Fahima Dilnawaz · Ranjita Misra · Anju Harilal · Rama Shenkar Verma · Sanjeeb K. Sahoo · Subramanian Krishnakumar

Abstract To develop a suitable formulation with high entrapment efficiency, etoposide-loaded poly(lactide-*co*-glycolide) nanoparticles (NPs) were formulated by single emulsion-solvent evaporation method by changing different formulation parameters such as drug loading, choice of organic solvent and percentage of emulsifier polyvinyl alcohol. The NPs showed higher entrapment efficiency, ~86% (with 15% (*w/w*) drug loading). The physicochemical parameters revealed smooth topology with size range (240–320 nm), a negative zeta potential (~19 mV) and in vitro sustained-release activity (~60% drug release in 40 days). Greater anti-proliferative activity ~100 times was observed with NPs ($IC_{50}=0.002$ μg/ml) than that of native etoposide ($IC_{50}=0.2$ μg/ml) in retinoblastoma cell line (Y-79). These NPs demonstrated greater (G1/S) blocking and decreased mitochondrial membrane potential as measured by flow cytometry. There was upregulation of apoptotic gene activity in NPs than native etoposide, as revealed through microarray analysis. However, this is the first ever report demonstrating the intricate modulation of genetic network affected by NPs. Collectively, these results suggest that etoposide-loaded NPs could be potentially useful as a novel drug delivery system for retinoblastoma in the future.

Keywords Retinoblastoma · Ocular drug delivery · PLGA nanoparticles · Apoptosis · Gene expression

Moutushy Mitra and Fahima Dilnawaz have equal contribution.

Electronic supplementary material The online version of this article (doi:10.1007/s12645-010-0010-4) contains supplementary material, which is available to authorized users.

M. Mitra · A. Harilal · S. Krishnakumar (✉)
Department of Ocular Pathology, Vision Research Foundation,
Sankara Nethralaya, No 18 College Road, Nungambakkam,
Chennai 600006, India
e-mail: drkrishnakumar_2000@yahoo.com

F. Dilnawaz · R. Misra · S. K. Sahoo
Institute of Life Sciences,
Nalco Square, Chandrasekharpur,
Bhubaneswar, Orissa, India

R. S. Verma
Indian Institute of Technology,
Madras, India

M. Mitra
CeNTAB, Sastra University,
Tanjore, India

1 Introduction

Retinoblastoma is the most common intraocular malignancy found during infancy and childhood (Rodriguez-Galindo et al. 2008), and it represents the phenotypic expression of abnormal or absence of tumour suppressor gene known as retinoblastoma gene (*RB1*; Friend et al. 1987). The protein product of the *RB1* gene (the retinoblastoma protein) regulates a cellular anti-proliferative Rb pathway. The deregulation of the *RB1* gene results in a spectrum of malignancies (Van Quill et al. 2005). Treatment options for retinoblastoma include external radiotherapy, episcleral plaque radiotherapy and cryotherapy (Amendola et al. 2006). However, these treatments are associated with complications such as facial deformities, cataract and radiation retinopathy and with a substantial risk for secondary tumours (Abramson et al. 1998; Smith and Donaldson 1991). Therefore, systemic chemotherapy treatment is the only options left for the widely used treatment of retinoblastoma. However, their clinical use is limited with systemic toxicity, rapid blood clearance and drug resistance (Chan et al. 2005; Travis et al. 1999). The presence of the blood retinal barrier further limits the potential

of various anticancer drugs. Therefore, ocular drug delivery is one of the challenging tasks faced by pharmaceutical scientists because of its critical and pharmacokinetically specific environment that exists in the eye (Sahoo et al. 2008).

As per the anatomical structure of the eye, the inner and outer blood retinal barriers separate the retina and vitreous from the systemic circulation to the vitreous body which reduces the movement of molecules, further limiting the potential of various anticancer drugs (Abramson et al. 2003). To increase the therapeutic index, nanotechnology is one of the potential approaches where cytotoxic drugs are encapsulated in nanoparticles to augment drug activity by maximizing drug availability, leading to the reduction of harmful effects of drug by minimizing drug exposure to healthy tissues. Harmia et al. (1986) encapsulated pilocarpin in poly(alkylcyanoacrylate) which are able to improve the intraocular penetration of drugs. Also, Calvo et al. (1996) formulated cyclosporine A polyester nanocapsules as a topical delivery system for improved ocular penetration of drugs. Similarly, Enríquez de Salamanca et al. (2006) developed chitosan-based nanocarriers as the potential vehicle for ocular delivery. However, all of the above studies demonstrated that these nanoparticles are well tolerated by the ocular surface tissues. These supportive facts further support the potential use of nanoparticles to deliver the drugs to the ocular surfaces.

Considering these points, the development of a drug delivery system is becoming increasingly important in the treatment of vitreoretinal diseases by facilitating the drug efficacy and attenuating the adverse effects whilst assisting their interaction with ocular tissues (Wong et al. 1987). Nanoparticles are polymeric colloidal particles with size ranging from 10 to 1,000 nm, in which the therapeutic agents of interest can be encapsulated or conjugated or adsorbed to its surface (Sahoo et al. 2008; Misra et al. 2009). Moreover, polymeric nanoparticles have been evaluated as ocular drug delivery systems to enhance the absorption of therapeutic drugs, improve bioavailability, reduce systemic side effects, and to sustain intraocular drug levels (Hashizoe et al. 1997; Marchal-Heussler et al. 1993; Zimmer et al. 1995). In addition, polymeric nanoparticles have been shown to have potential in the treatment of inflammatory external eye diseases (Diepold et al. 1989). Poly(lactide-co-glycolide) (PLGA) is a copolymer of poly(D,L-lactide-co-glycolide) and is an ideal candidate of biodegradable polymers for formulation into nanoparticles due to its wide medical use, biocompatibility and safety (Yasukawaa et al. 2004).

Etoposide is an anticancer drug used in the treatment of a variety of malignancies including malignant lymphomas, acute myeloid leukemia, lung cancer, Hodgkin's disease, non-Hodgkin's lymphoma, AIDS-related Kaposi's sarcoma, gastric cancer, breast cancer and ovarian cancer (Hande 1992; Smit et al. 1989). It acts by inhibiting topoisomerase-II and activating oxidation/reduction reactions to produce derivatives that bind directly to DNA and cause DNA damage (Ashley et al. 1996). Effective cancer therapy for tumours precisely depends on continuous exposure of the anticancer agents for a prolonged period of time, which is not possible due to the short biological half-life (190 min) of etoposide (Reddy et al. 2006). Etoposide, being a hydrophobic drug, possesses a dissolution-related absorption problem because of poor aqueous solubility and bioavailability (Shah et al. 1995). Snehalatha et al. (2008) have reported the high significance and advantage of PLGA and PCL nanoparticles as drug carriers for etoposide with enhanced bioavailability and reduced etoposide-associated toxicity in rabbits and mice. Similarly, Yadav and Krutika (2010) have developed a sustained-release formulation of etoposide for continuous intravenous administration replacing the conventional therapy. They have reported that nanoparticles (NPs) remained stable in terms of both size and drug content for a longer period of time. Therefore, it is of enormous interest to develop a formulation which can overcome the solubility and related bioavailability problems of etoposide as a therapeutic agent particularly for the treatment of retinoblastoma.

We propose here that the diverse side effects of etoposide can be significantly reduced by encapsulating the drug in the nanoparticulate system. In the present investigation, etoposide-loaded NPs were formulated to achieve a high entrapment efficiency of etoposide by varying different parameters like organic solvent, per cent of drug loading (w/w) and the amount of polyvinyl alcohol (w/v). We selected the best suitable formulation with optimum size range and higher encapsulation efficiency for further studies. The nanoparticles were characterized in terms of their particle size, zeta potential, surface morphology and entrapment efficiency by different techniques. We have studied the cytotoxicity, cellular uptake (qualitative and quantitative), induction of apoptosis and modulation of mitochondrial permeability by these nanoparticles using the Y-79 cell line, and these results were compared with native etoposide. Moreover, the NPs were further evaluated for the regulation of different apoptotic gene activities in the retinoblastoma cell line by microarray technique.

2 Materials and methods

2.1 Materials

Poly(D,L-lactide-co-glycolide) (copolymer ratio 50:50, viscosity 0.55–0.75) was purchased from Birmingham Polymers Inc. (Birmingham, USA); propidium iodide (PI) from MP, Biomedicals, Inc. (Germany); AnnexinV-FITC from Biosciences, Pharmigen; Pierce BCA Protein Assay Kit (Rockford, IL, USA); and uranyl acetate from Electron Microscopy Sciences (Hatfield, PA, USA). Polyvinyl

alcohol (PVA, average M_w 31,000–50,000), etoposide, 6-coumarin, Tween 80 (polyoxyethylene sorbitan monooleate), Igepal CA-630, MTT (3-(4,5-dimethylthiazol-2-yl)-2,5-diphenyl tetrasodium bromide) reagent and different salts were purchased from Sigma-Aldrich Co. (St. Louis, MO, USA). All other chemicals used in this study are of analytical grade from E Merck (India). Uranyl acetatae was from Electron Microscopy Services, Ft. (Washington, PA, USA) and carbon-coated copper TEM grid (150-mesh) from Ted Pella Inc. (Rrodding, CA, USA).

2.2 Preparation of etoposide-loaded nanoparticles

The NPs were prepared by single emulsion-solvent evaporation technique (Sahoo et al. 2004a). Briefly, 90 mg of PLGA was dissolved in 3 ml of chloroform or dichloromethane. To the above mixture, either 10% or 15% (w/w) etoposide was added and emulsified with 12 ml of either 2% or 5% (w/v) aqueous solution of PVA. The emulsification was carried out using a microtip probe sonicator (VC 505, Vibracell Sonics, Newton, USA) at 39 W of energy for 2 min in an ice bath and stirred with a magnetic stirrer overnight to evaporate the organic solvent. The NPs were recovered by ultracentrifugation at 40,000 rpm for 20 min at 4°C (Sorvall Ultraspeed Centrifuge, Kendro, USA), followed by washing twice with double distilled water. The obtained particles were resuspended in double distilled water and lyophilized (−80°C and <10-µm mercury pressure, LYPHLOCK 12, Labconco, Kansas City, MO, USA) for 48 h. Lyophilization is required for longer storage and stability of these nanoparticles which can be stored at 4°C for further experiments (Lemoine et al. 1996). To study the cellular uptake of NPs, 6-coumarin was used as a model fluorescent probe. To formulate 6-coumarin-loaded nanoparticles, 50 µl (1 mg/ml) of dye (dissolved in methanolic/chloroform, 12.5:87.5, v/v) was added to the polymer solution prior to emulsification instead of etoposide formulation.

2.3 Determination of encapsulation efficiency by RP-HPLC

To estimate the amount of drug entrapped inside the NPs drug content, 10 mg of etoposide nanoparticles was dissolved in 10 ml of methanol, sonicated in an ice bath for 1 min at 39 W (VC 505, Vibracell Sonics) and centrifuged at 13,800 rpm for 10 min at 25°C (Sigma1-15K, Germany). The supernatant was estimated by the reverse phase isocratic mode of HPLC with slight modification (Shirazi et al. 2001): Agilent 1100 (Agilent Technologies, Waldbronn Analytical Division, Germany), featured with C18 column (Zorbax Eclipse XDB-C18,150×4.6 mm, i.d), quaternary pump (model no. G1311A), thermostart (model no. G1316A) and a diode array detector (model G 1315A). Twenty microlitres

of the sample was injected manually in the injection port and analysed with a flow rate 1 ml/min at 60°C with UV detection at 220 nm using the mobile phase of methanol/water (45:55, v/v). The standard curve of etoposide was prepared under identical condition. The encapsulation efficiency (%) was determined as the percentage of drug entrapped in nanoparticles with respect to the initial amount of drug added in the formulation (Sahoo et al. 2004a).

2.4 Physicochemical characterization of nanoparticles

Particle size, size distribution and zeta potential of the etoposide nanoparticles were determined by photon correlation spectroscopy and laser Doppler anemometry, respectively, using Zetasizer (Nano ZS, ZEN 3600, Malvern Instrument, UK) with a red laser of wave length $\lambda_0 = 633$ nm (He–Ne, 4.0 M_w). For the above measurement, the lyophilized nanoparticles were suspended in double distilled water and sonicated to get a homogenous suspension. The acquired suspension was examined for mean diameter, size distribution, polydispersity and zeta potential. Scanning electron microscopy (Hitachi S-3400N, USA) was used to determine the shape and surface morphology of the nanoparticles. The powdered particles were gold-coated and vacuum-dried before scanning electron microscopy (SEM). For the transmission electron microscopy (TEM, Philips CM-10, FEI Inc., Hillsboro, OR, USA), a drop of diluted and sonicated solution of nanoparticle was negatively stained with 1% uranyl acetate for 10 min, placed in carbon-coated copper TEM grid and air-dried before TEM. Fourier transform infrared spectroscopy (Perkin Elmer model Spectrum1, USA) measurement was done to determine the possible chemical interaction between the drug and the polymer. The samples (native etoposide, void NPs and NPs) were crushed individually with KBr to get the pellets by applying a pressure of 300 kg/cm^2, and the spectra scanned were obtained in the range between 4,000 and 500 cm^{-1} using IR solution software (version 1.10). Differential scanning calorimetry (DSC 821, Mettler Toledo, Switzerland) technique was implemented to determine the physical state of the encapsulated etoposide in nanoparticles. Each sample (native etoposide, void nanoparticles and etoposide nanoparticles) was sealed separately in a standard aluminium pan, purged with pure dry nitrogen with a flow rate of 10 ml/min, at 10°C/min, and heat flow recorded from 0°C to 350°C.

2.5 In vitro release of etoposide from nanoparticles

The release of drugs from nanoparticles was carried out in phosphate-buffered saline (PBS, 0.01 M, pH 7.4, containing 0.1% (w/v) of Tween 80) in triplicates (Sahoo et al. 2004a).

In brief, 10 mg of nanoparticles was dispersed in 3 ml of PBS, sonicated (30 s) and equally distributed into three tubes. Then, the tubes were placed in an orbital shaker bath (Wadegati Lab Equip, India) maintained at 37°C and with horizontal rotation at 150 rpm. At predetermined time intervals, the tubes were taken out of the shaker and centrifuged at 13,800 rpm for 10 min at 4°C (Sigma Microcentrifuge 1-15K, Germany). The entire supernatant was collected for further analysis. The residue pellet was resuspended with fresh PBS and placed back into the shaker to continue the release measurement. The collected supernatants were lyophilized for 48 h, dissolved in methanol for the dissolution of the drug and centrifuged at 13,800 rpm for 10 min. The obtained supernatant was subjected to RP-HPLC analysis to determine the amount of etoposide released as described above.

2.6 Quantitative cellular uptake of nanoparticles

Cellular uptake efficiency of cells was studied using 6-coumarin-loaded nanoparticles. For this, the cells were seeded at 5×10^4 per well density in 24-well plates (Corning, NY, USA) and left 24 h for attachment; thereafter, cells incubated for 2 h with 300 μg/ml of 6-coumarin-loaded nanoparticles and equivalent concentration of native 6-coumarin. After the incubation period, the cells were washed thrice with PBS (0.1 M, pH 7.4) and lysed by incubating them with 0.1 ml of 1× cell lysis reagent (Igepal CA-630, Sigma-Aldrich) for 30 min at 37°C. From which, 5 μl was taken out for the cell protein estimation using the Pierce BCA protein assay. The remaining cell lysate was lyophilized. The dye from the lyophilized nanoparticles was extracted by dissolving each sample with 1 ml of methanol/chloroform (12.7:87.5, v/v) solution and kept in a shaker at 37°C for 48 h at 150 rpm/min in an orbit shaking incubator (Wadegati Labequip, India) for the complete removal of the dye from the NPs. The samples were then centrifuged at 13,800 rpm for 10 min at 4°C and the supernatants collected. Fluorescence intensity of the supernatants was measured by a fluorescent spectrophotometer (Synergy HT, BioTek® Instruments, Inc., Winooski, VT, USA) at $\lambda_{ex} = 450$ nm and $\lambda_{em} = 490$ nm. A standard plot of 6-coumarin nanoparticles (2–50 μg/ml) was constructed in a similar way to determine the amount of nanoparticles in the cell lysate. The uptake of nanoparticles by cells was calculated from the standard plot and expressed as the amount of nanoparticles (μg) taken per milligram cell protein.

2.7 Cytotoxicity assay

A comparison of the cytotoxic activity of NPs and native etoposide was performed using the MTT assay as described earlier (Sahoo et al. 2004b). Y-79 cells were plated in 96-well plates (Corning) at a density of 5,000 cells/well incubated for 24 h for cell adherence. A stock solution of etoposide was prepared in DMSO (1 mg/ml) and stored at −70°C. Different aliquots of the stock solution after suitable dilution were added to the culture medium to achieve the desired drug concentration. The concentration of DMSO in the medium was kept 0.1% so that it has no effect on the cell proliferation. Cells were incubated with different concentrations of etoposide either as solution or encapsulated in NPs. Medium and void nanoparticles (without drug) served as respective controls. The medium was changed on every alternate day and no further dose of the drug was added. The cell viability was determined at the fifth day following drug treatment using the MTT reagent. Ten microlitres of the MTT solution was added to each well and incubated at 37°C for 3 h in a cell culture incubator. The medium was removed and replaced with 100 μl of DMSO to dissolve formazan crystals; absorbance was read at 540 nm using a microplate reader (Synergy HT, BioTek® Instruments, Inc.). The anti-proliferative effects of different treatments were calculated as a percentage of cell growth with respect to the respective controls. IC_{50}, the concentration of the drug at which 50% cell growth is inhibited, was calculated by the curve fitting of the cell viability data using Prism 4.0 (GraphPad, San Diego, CA, USA).

2.8 Cell cycle analysis

The distribution of DNA in the cell cycle was studied by flow cytometry. Cell cycle analysis of native etoposide and etoposide-loaded nanoparticles was done with slight modification (Noh et al. 2004). Briefly, 5×10^5 cells/5 ml were seeded in T-25 flask (Corning) and incubated overnight for better attachment. The cells were exposed to a particular concentration (0.0005 μg/ml) of drug in solution, drug-loaded nanoparticles in RPMI medium, and incubated for 48 and 120 h. Void nanoparticle-treated cells and untreated cells were used as respective controls. The cells were collected and washed with PBS (0.1 M, pH 7.4) twice and resuspended in hypotonic propidium iodide solution (10 μg of propidium iodide, 10 μg of RNase A and 0.5% "Tween 20 in 1 ml of PBS) for 1 h at room temperature and kept in the dark at 4°C before analysis. Cell cycle distribution was determined by analysing 10,000 cells using FACScan flow cytometer and Cell Quest software Caliber (Becton-Dickinson, San Jose, CA, USA). All experiments were performed in triplicate.

2.9 Mitochondrial membrane permeability study

Mitochondrial membrane depolarization study was done using flow cytometry (Raffaella et al. 2005). Briefly, 5×10^5 cells per well were seeded and incubated overnight. The cells were exposed to a particular concentration (0.0005 μg/ml)

of native etoposide and etoposide-loaded nanoparticles for 5 days. The medium was changed in every alternate day. Cells were stained with the cationic dye 5,5,6,6 tetrachloro-1,1,3,3-tetraethylbenzimidazol-carbocyanine iodide (JC-1, 3 μg/ml) for 10 min at 37°C, which exhibits potential-dependent accumulation in mitochondria. The cells were washed with PBS (0.1 M, pH 7.4) twice and analysed using FACScan flow cytometer and Cell Quest software Caliber (Becton-Dickinson). All experiments were performed in triplicate.

2.10 Assessment of apoptosis

Annexin V-FITC staining was used for the assessment of apoptosis. This assay is based on the observation that soon after the initiation of apoptosis, phosphotidylserine (PS) translocates from the inner face of the plasma membrane to the cell surface. The translocated PS can thus be easily detected by staining with a FITC conjugate of Annexin V, a protein that has a strong natural affinity for PS (Martin et al. 1995). In our experiments, 1×10^6 cells/well were cultured on six-well plates (Corning) in 3 ml medium; 24 h post-seeding, they were treated with two different concentrations (0.0005 and 0.005 μg/ml) of the native drug and etoposide-loaded nanoparticles, and 5 days after treatment, the cells were collected from the wells, centrifuged, washed thrice with PBS (0.01 M, pH 7.4) and incubated for 15 min in the dark in 100 μl of binding buffer containing 2 μg/ml Annexin V-FITC (BD Biosciences Pharmingen) and 10 μg/ml of the vital dye, propidium iodide (MP Biomedicals, Inc., Germany). Thereafter, the cell suspension was placed on a glass slide, covered with a glass coverslip and photographed using a fluorescence microscope (Nikon Fluorescence, Nikon, Japan) equipped with blue, red and green filter attachment. The apoptotic index was obtained by dividing the number of apoptotic cells by the total number of cells, multiplied by 100 (Rödel et al. 2003). A minimum of 1,000 cells were counted using an image analyzer.

2.11 DNA fragmentation studies by gel electrophoresis

DNA fragmentation into oligonucleosomal ladder is a characteristic of apoptosis. To study this, 1×10^6 cells per well were seeded in six-well plate (Corning) and after 24 h were then treated with two different concentrations (0.0005 and 0.005 μg/ml) of the drug either as a solution or encapsulated in nanoparticles. Medium and void nano-particles served as respective controls. After 5 days of post-treatment, cells were collected, washed and centrifuged at 2,500 rpm for 5 min. The cell pellet was lysed with 0.1 ml of 1× cell lysis buffer (Igepal CA-630, Sigma-Aldrich) and incubated for 30 min at 37°C; after, 2 μl of 10 μg/ml RNase was added and incubated for a further 1 h. The obtained cell lysate samples of 20 μl/well were subsequently run at 120 V on a 1% (w/v) agarose gel containing 0.1 mg/ml ethidium bromide. Gels were examined on an ultraviolet light source and photographed.

2.12 Statistical analysis

Statistical analyses were performed using a Student's t test of the software, and the differences were considered significant for p values of <0.05* and <0.005**.

3 Results and discussion

3.1 Physicochemical characterization of nanoparticles

NPs were prepared by single emulsion-solvent evaporation technique. The particle size (hydrodynamic diameter) of nanoparticles observed by dynamic laser light scattering (DLS) technique revealed their size in the range of 240–320 nm (Table 1). Figure 1a depicts the size of the NPs observed by the DLS. The smooth and rounded shape topology of the nanoparticles was confirmed by SEM (Fig. 2b) and internal diameter of ~200 nm, as observed from TEM (Fig. 1c). The particle size measurement by DLS is higher than that of TEM measurement because DLS measures the apparent size, including the hydrodynamic layers formed due to hydrophilic coating around the nanoparticles, thus leading to overestimation of the size (Acharya and Sahoo 2009) as particle size is an important parameter and has a direct relevance with the stability, cellular uptake, drug release and biodistribution (Panyam et al. 2004). Concerning this, we have studied the influence of different formulation parameters such as the organic solvent (dichloromethane or chloroform) and the amount of emulsifying agent (e.g. PVA) on particle size NPs, as depicted in Table 1. The results demonstrated that the particle size was larger in chloroform than dichloromethane irrespective of the amount of drug loading (Table 1). The slight decrease in particle size using dichloromethane as solvent may be due to the miscibility of dichloromethane with the aqueous phase used in formulation than that of chloroform as dichloromethane is soluble in ~50 parts of water, whereas chloroform is soluble in ~200 parts of water (Table 2). The acquired data clearly indicated the influence of the physical properties of the organic solvent in the physicochemical properties of the nanoparticles due to the fact that PVA partitioned into the polymeric phase containing an organic solvent that is more miscible with the aqueous phase, forming smaller emulsion droplets; as a result, there was a decrease in nanoparticle size in the case of dichloromethane-mediated formulation (Sahoo et al. 2002). Furthermore, the concentration of PVA also influenced the size of nanoparticles (Sahoo et al. 2002).

Table 1 Comparative analysis of encapsulation efficiency, size and zeta potential of etoposide-loaded nanoparticles

PVA (%)	Drug loading (%, w/w)	Organic solvent	Encapsulation efficiency (%)[a]	Mean diameter (nm)[b]	Zeta potential (mV)[c]
2	10	$CHCl_3$	61	316±1.5	−14±0.9
–	15	–	80	322±1.1	−14±0.9
–	10	CH_2Cl_2	41	299±1.1	−17±1.1
–	15	–	55	305±0.9	−19±1.2
5	10	$CHCl_3$	60	267±1.2	−20±1.3
–	15	–	86	270±1.0	−19±1.6
–	10	CH_2Cl_2	56	247±1.2	−24±1.8
–	15	–	72	251±1.1	−22±1.2

[a] Encapsulation efficiency of the etoposide-loaded nanoparticles

[b] Size (in nm) as measured by dynamic laser scattering method

[c] Zeta potential (in mV) as measured by zetasizer

Therefore, we studied the effects of different PVA concentrations (2% and 5%) in the external aqueous phase on the particle size. With the increase of PVA concentration in the external aqueous phase, the mean nanoparticle size also decreased irrespective of the use of organic solvent and percentage of drug loading (Table 1). This might be due to the more number of PVA molecules oriented at the organic solvent/water interface to reduce the interfacial tension during emulsification, which prevents nanoparticle aggregation during the process of organic solvent evaporation (Sahoo et al. 2002). The formulated NPs showed negative surface charge attributed to the presence of ionized carboxylic groups on the surface of the nanoparticles in the range of −14 to −25 mV, as depicted in Table 1.

Apart from the smaller size, the successful implementation of nanoparticles as drug delivery vehicles requires a higher drug loading efficiency. Therefore, we have used 10% or 15% (w/w) drug loading corresponding to the polymer weight (Table 1). We achieved higher encapsulation efficiency in the case of 15% (w/w) drug loading irrespective of the organic solvent and concentration of emulsifier. An increased encapsulation efficiency up to ~86% was achieved using chloroform as organic solvent, whereas using dichloromethane, the encapsulation efficiency reached up to ~72%. The slightly hydrophilic nature of dichloromethane leads to a slightly lower entrapment efficiency with smaller particle size, whereas the less hydrophilic nature of chloroform leads to higher entrapment efficiency with a slightly bigger particle size. This could happen probably due to more accommodation of drug molecule in the polymeric surface due to drug–polymer interaction (Panyam and Labhasetwar 2004). Besides, the polarity behaviour of the organic solvent (Table 2) also might have affected the entrapment efficiency during the nanoparticle formulation. Therefore, in our formulation, we established chloroform to be a more suitable solvent than dichloromethane for the encapsulation of the hydrophobic drug etoposide (Table 1).

3.2 FT-IR analysis

Fourier transform infrared spectroscopy (FT-IR) spectral analysis was exercised to determine any possible chemical interaction (formation of chemical bonds) that occurred in the polymer due to the addition of drug during the synthesis process (Misra et al. 2009; Vandana 2009). Figure 2 depicted the FT-IR spectra of void nanoparticles, native etoposide and NPs. The spectra of NPs showed the presence of bands similar to void NPs along with some extra bands due to the drug. The vibrational spectral analysis of native etoposide illustrated characteristic bands due to different functional groups such as 3,450, 2,892, 1,769, 1,615,1,459, 1,390 and 1,161 cm^{-1}, corresponding to OH, $-CH_2$ stretching, lactone group, aromatic groups, –
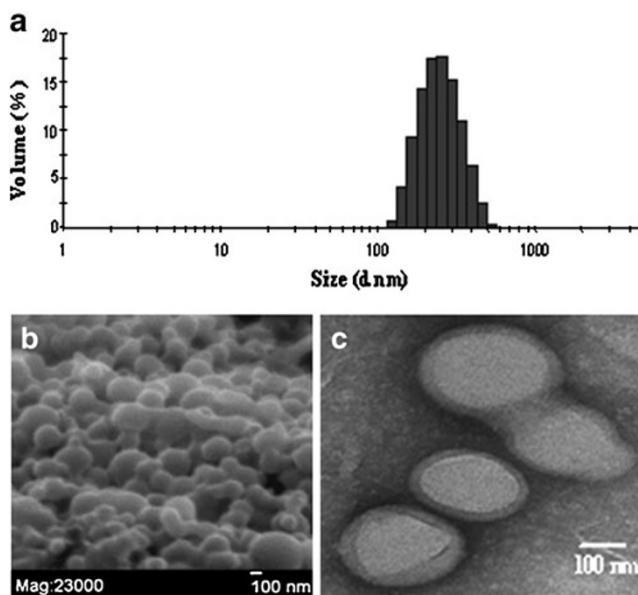
Fig. 1 a Measurement of size distribution of NPs through particle size analyzer. **b** SEM of NPs. **c** TEM of NPs
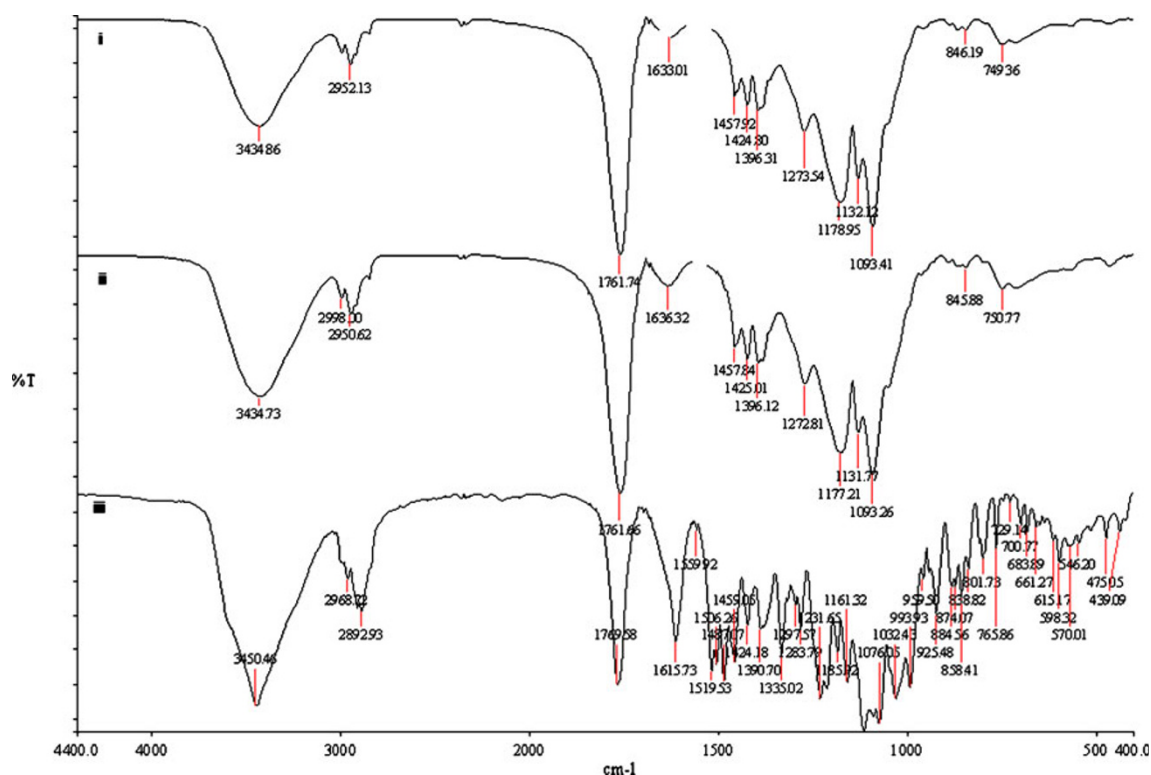
Fig. 2 FT-IR spectra of void nanoparticles (*i*), native etoposide (*ii*) and etoposide-loaded nanoparticles (*iii*)

OH, –C–O from –OCH$_3$ and AROH functional groups, respectively. Similar types of bands were also observed earlier (Jasti et al. 1995). However, the vibrational spectral peaks of drugs at 3,450, 2,892 and 1,769 cm^{-1} are slightly displaced to 3,434, 2,998 and 1,761 cm^{-1} in NPs due to some minor chemical interaction between etoposide and the PLGA matrix. Moreover, the band appearing at 1,769 cm^{-1} in native etoposide also appeared in NPs with increased intensity, indicating the presence of negligible chemical interaction with the polymer. However, such chemical interaction has no significant effect on the in vitro release profile of drug. Similar chemical integrity and chemical stability of doxycycline drug inside the nanoparticles were also studied through FT-IR analysis (Misra et al. 2009).

3.3 DSC studies

DSC study was performed to determine the nature of the encapsulated drug inside the NPs. The DSC results revealed the amorphous nature of the encapsulated drug. Through DSC analysis, the endothermic peak of the PLGA polymer was observed at 54°C as PLGA exhibited a glass transition temperature (T_g) at ~54°C. The endothermic peak of native etoposide was found approximately at 189°C (Fig. 3). This characteristic peak was not observed in NPs, which indicated that the encapsulated drug in nanoparticles is in amorphous or disordered-crystalline phase in the polymer matrix, resulting in the molecular dispersion of the drug inside the nanoparticles (Misra et al. 2009).

3.4 In vitro release profile of nanoparticles

The release profile of etoposide from the nanoparticles was studied in vitro using PBS (0.01 M, pH 7.4). A typical two-phase release profile was observed, as depicted in Fig. 4 which demonstrated a relatively rapid release in the early time point (~ 28% of the entrapped etoposide release in 72 h) followed by sustained and slow release over a

Table 2 Physical properties of the solvents

Solvent	Boiling point (°C)	Melting point (°C)	Solubility in water at 25°C	Interfacial tension (dyne/cm)	Viscosity (Cp)
Dichloromethane	39.75	−95	1 in 50	28.3	0.44
Chloroform	61–62	−63.5	1 in 200	32.8	0.57

Data as taken from Sahoo et al. (2002)
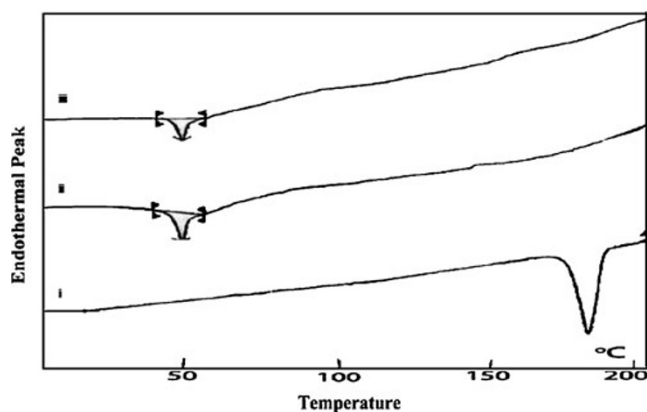
Fig. 3 Differential scanning calorimetry thermogram curves of native etoposide (*i*), void nanoparticles (*ii*) and NPs (*iii*)

prolonged time period (~60% of the drug released in 6 weeks). The release of a drug from the polymeric nanoparticles is a rather complicated process (Reddy et al. 2006; Panyam and Labhasetwar 2004). The initial release of etoposide might be due to the rapid release of drugs deposited on the surface along with the formation of water channels in nanoparticles. Since the degradation of PLGA is slow, at a later stage, the release of etoposide from the nanoparticles primarily depends on the drug diffusion and degradation of the polymer matrix itself (Panyam and Labhasetwar 2003).

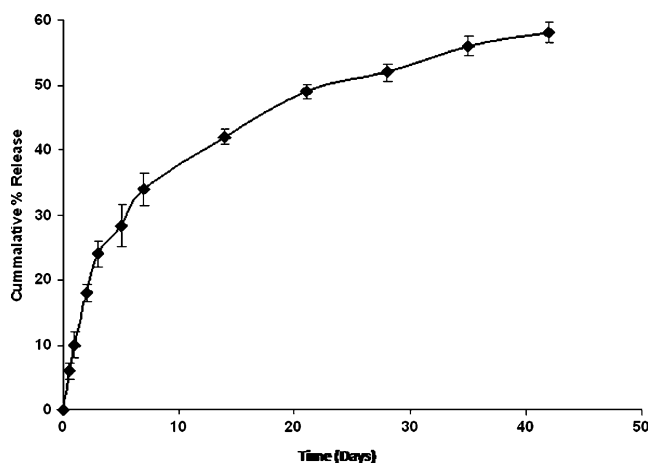### 3.5 Cellular uptake of native 6-coumarin and 6-coumarin-loaded nanoparticles

The photoluminescent behaviour of 6-coumarin has been recognized as a useful tool for the cellular uptake study of non-fluorescent drug molecules through fluorescence/confocal microscopy (Davda and Labhasetwar 2002). The intracellular uptake of 6-coumarin-loaded nanoparticles and native 6-coumarin was examined in Y-79 cells quantitatively by fluorescence spectroscopy. Cellular uptake studies illustrated that 6-coumarin-loaded nanoparticles were internalized more in comparison with native 6-coumarin (Fig. 5a). It was observed that the cellular uptake of 6-coumarin-loaded nanoparticles were internalized approximately sevenfold higher as compared with native 6-coumarin. This might be attributed to the fact that the entry of the dye-loaded nanoparticles into the cells is via endocytosis as compared with the entry of native 6-coumarin by a passive diffusion mechanism (Sahoo and Labhasetwar 2005). The studies of Qaddoumi et al. (2003) revealed that the uptake of the PLGA nanoparticles in primary culture of rabbit conjuctival epithelial cells occurred through endocytosis. Other independent observation of the endocytic uptake of the nanoparticles was also reported (Acharya and Sahoo 2009). The higher cellular uptake of the nano-

particulate formulation versus native 6-coumarin could be explained on the basis of the increased cellular accumulation of the encapsulated dyes. The endocytic uptake of the colloidal nanoparticles was also revealed by independent studies (Enríquez de Salamanca et al. 2006; Douglas et al. 2008). Our studies evidently demonstrated the significance of the use of nanoparticles as a potential system compared to the free drug due to the enhanced drug retention and greater intracellular uptake for improved therapeutic efficacy.

We have studied the intracellular uptake of nanoparticles by confocal microscopy. The cells exposed to nanoparticles demonstrated increased fluorescence activity. Maximum fluorescence activity was observed in cells exposed to 6-coumarin-loaded nanoparticles, which indicated that nanoparticles were internalized more by the cells than native 6-coumarin (Fig. 5b). The fluorescence intensity of native 6-coumarin decreased with increased incubation time, i.e. 2, 24, 48 and 120 h. But in the case of 6-coumarin-loaded nanoparticles, the fluorescence intensity increased with increased time of incubation, signifying that the nanoparticulate formulation might act as an intracellular depository to maintain a sustained release of the dye from nanoparticles.

### 3.6 Cytotoxicity studies of native drug and nanoparticles

The therapeutic efficacy of drug-loaded nanoparticles would mostly depend on nanoparticle uptake, their intracellular distribution and, more notably, on the dose of the drug that is released from the internalized nanoparticles inside the cell (Acharya and Sahoo 2009). To investigate the induction of therapeutic efficiency of the formulations, Y-79 cells were treated with native etoposide, void nanoparticles (without drug) and NPs at


Fig. 4 In vitro release profile of etoposide from nanoparticles in PBS (0.1 M, pH 7). Data are as the mean ± SEM (*n*=3)

Fig. 5 **a** Cellular uptake of native 6-coumarin and 6-coumarin-loaded nanoparticles in Y-79 cells at 37°C. Data are represented as the mean ± SEM ($n=6$). **$p<0.005$, 6-coumarin-loaded nanoparticles versus native 6-coumarin. **b** Confocal fluorescence images highlighting time-dependant intracellular uptake of native 6-coumarin and 6-coumarin-loaded nanoparticles. *Scale bar*, 30 mm
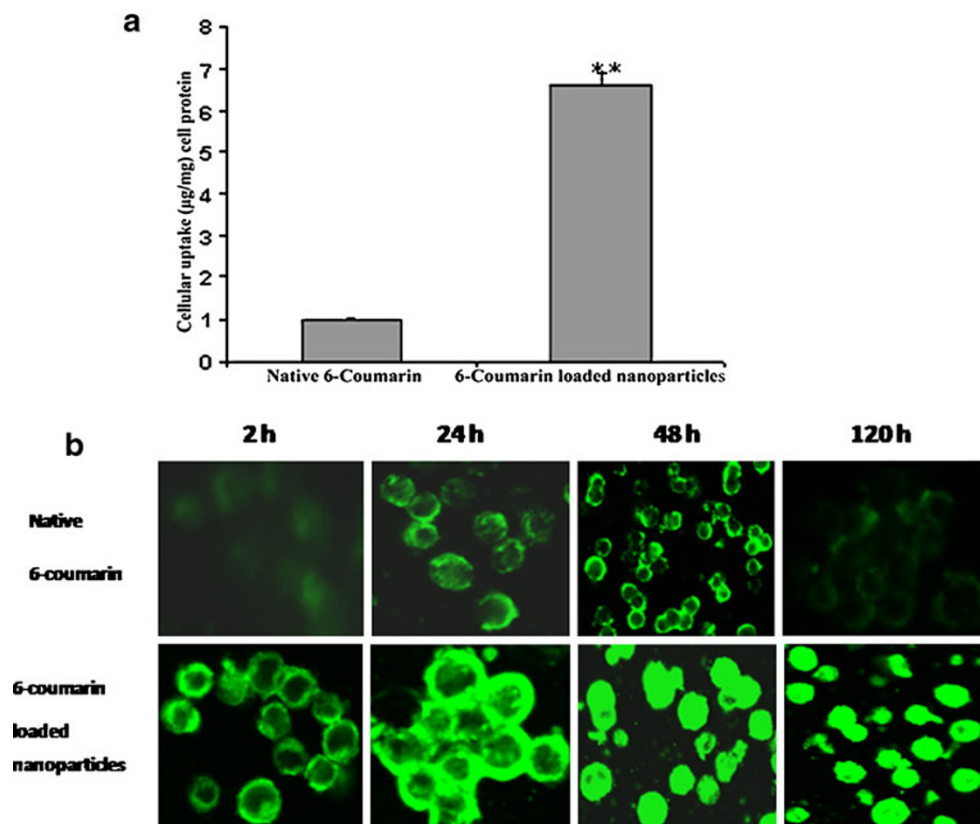
different concentrations for 5 days, and cell proliferation was measured by a standard MTT colorimetric assay. In vitro cytotoxicity studies exhibited the void nanoparticles to be nontoxic, which is similar to the medium with cells serving as control (data not shown), whereas the NPs demonstrated higher anti-proliferative activity than native etoposide (Fig. 6). Observation from IC_{50} values indicated the 100 times superior anti-proliferating efficiency for NPs (0.002 μg/ml) than that of native drug (0.21 μg/ml). The higher anti-proliferative activity could be attributed to the higher uptake of the nanoparticulate formulation, which leads to the accumulation and sustained release of the drug for a prolonged period of time at the site of action. Similar reports were observed with podophyllotoxin-loaded nanoparticles (etoposide is a derivative product of podophyllotoxin) on HeLa cells. Podophyllotoxin-loaded solid lipid nanoparticles (PDP-SLN) were formulated and its anti-proliferative activity was observed with MTT assay in HeLa cells. PDP-SLN showed effective anti-proliferation activity with lower a IC_{50} value of 0.2 μm/l than native podophyllotoxin, IC_{50} value around 1.3 μm/l (Shi et al. 2008). This might probably be the reason why the drug-loaded nanoparticles are internalized more into the cells and escape the multiple drug resistance barriers (Shi et al. 2008; Garcion et al. 2006). Apart from that, the polymeric envelope protects and prevents the drug degradation from the
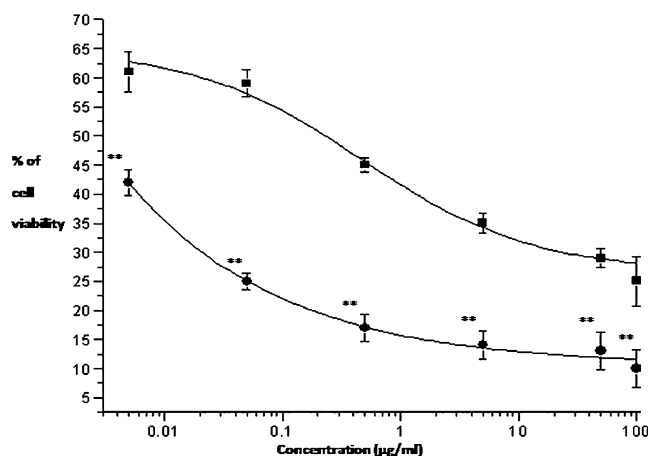
Fig. 6 Dose-dependent cytotoxic effect of etoposide in solution and in NPs. Different concentrations of etoposide either as solution (*black square*) or encapsulated in nanoparticles (*black circle*) were added to the wells. The medium was changed on the second day and fourth day with no further additional dose of drug. The extent of growth inhibition was measured on the fifth day by the MTT assay. The nanoparticles (without drug) or medium acts as respective controls. The percentage of survival was determined by standardizing the absorbance of controls to 100%. Data as ±SEM ($n=6$). **$p<0.005$ NPs versus etoposide solution

harsh internal environment, hence providing the concentration gradient for influxing of the drug in the cell. Whereas the native drug in the form of solution is vulnerable to all such conditions and degrades early as a result, it is not able to show the required anti-proliferative effect. Therefore, the higher efficacy of etoposide in NPs than the native etoposide in solution is due to the continuous exposure and sustained release of the drug for a prolonged period of time.

3.7 Cell cycle analysis of native drug and nanoparticles

Different drugs are known to have a range of pharmacological actions, including their effect on genes controlling the cell cycle and stimulation of pro- and antiapoptotic genes, and inhibition of secretion of various growth factors and cytokine-promoting inflammation (Panyam and Labhasetwar 2004). Etoposide inhibits cell growth and proliferation primarily through its effect on the cell cycle arrest and initiation of apoptosis (Shah et al. 1995). Void nanoparticle had no effect on cell cycle progression as compared to native cells and thus is nontoxic in nature. Figure 7a, b illustrated that incubating cells with NPs up to 48 h, maximum (61%) G1/S blocking occurred as compared with native etoposide (52%). The hypodiploid peak (sub-G1) appearing before the G1

phase on the histogram is called the apoptotic peak (Misra and Sahoo 2010), which indicates reduced DNA content in apoptotic cells in flow cytometry analysis. After 120 h of incubation, maximum percentage of apoptotic cells (12%) was found in the sub-G1 phase, which resulted in lesser proportion of G1/S (57%) blocking as compared with 48 h of incubation, whereas native etoposide showed comparatively lower apoptotic cells (9%) and G1/S blocking (46%). These results represented that with 48 h of incubation with NPs, which first leads to cell cycle inhibition and afterwards with increased time of incubation, the nanoparticles supplemented sustained release of drugs, which resulted in apoptosis. The above results can be easily corroborated with our 120 h of DNA fragmentation study.

3.8 Assessment of apoptosis by mitochondrial permeability/ Annexin V-FITC and DNA fragmentation method

Changes in mitochondrial membrane potential were analysed using a flow cytometer by using a mitochondria-selective dye, JC-1. The cationic dye JC-1 exhibits potential-dependent accumulation in the mitochondria, indicated by a fluorescence shift from green (~529 nm) to orange (~590 nm), due to the concentration-dependent intramitochondrial formation of
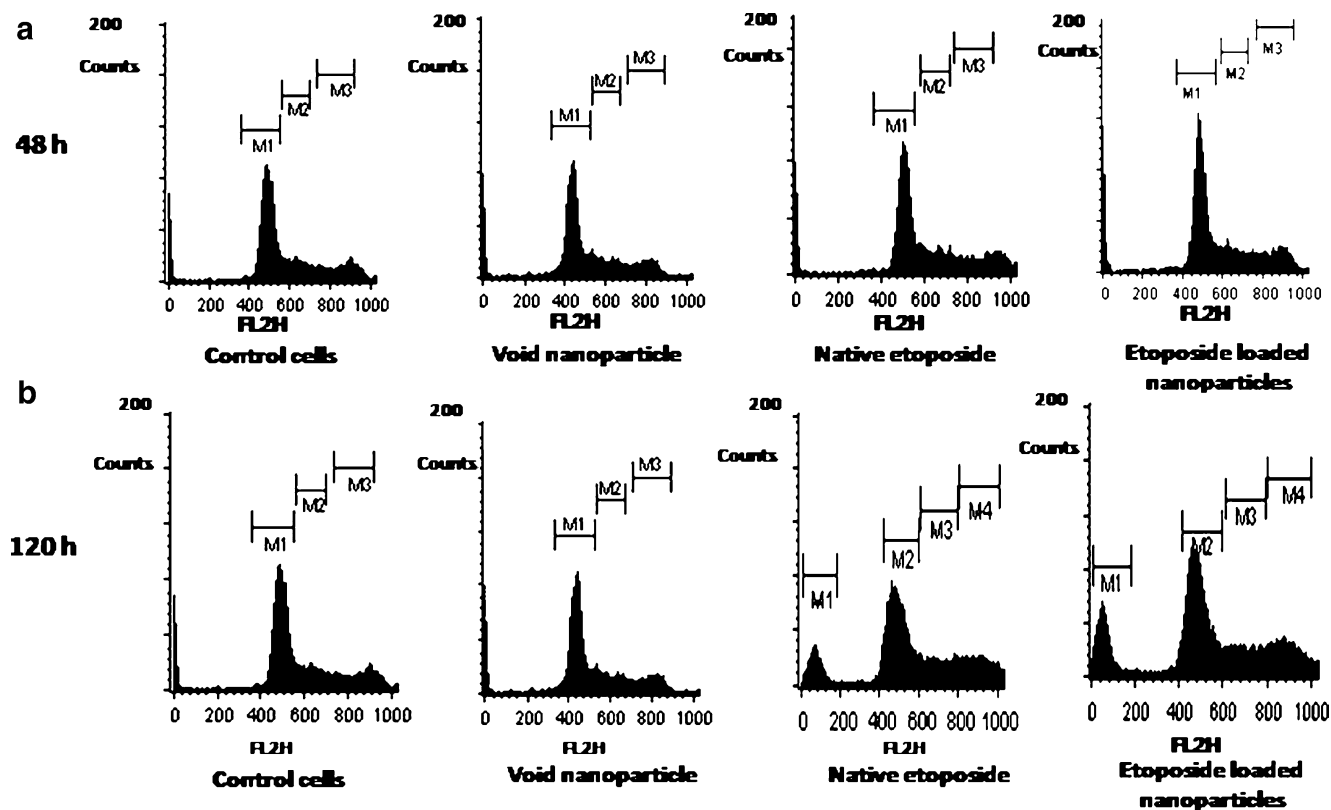
Fig. 7 Effect of native etoposide and NP treatments on cell cycle distribution in Y-79 cells. Cell cycle distribution was determined by analysing 10,000 ungated cells using FACScan flow cytometer. Content of DNA is represented on the x-axis; number of cells counted is represented on the y-axis (n ¼ 3). a Cells incubated for 48 h. b Cells incubated for 120 h

orange fluorescent oligomers. As a consequence, the changes in the mitochondrial membrane potential ($\Delta\psi_m$) can be optically measured by the orange/green fluorescence intensity ratio occurring during the process of apoptosis. During the apoptotic event, firstly, the mitochondria provide energy in the form of ATP, requisite for cells to die by the apoptotic pathway, and eventually release proapoptotic proteins into the cytosol to trigger the downstream apoptotic signalling pathways. The flow cytometry analysis (Fig. 8a, b) showed that NPs (0.0005 µg/ml) induced a decreased in dye uptake, indicating loss of $\Delta\psi_m$. The mitochondrial membrane potential decreased by 4.4% in 48 h and 8.8% in 120 h, thus demonstrating that NPs disturbed the mitochondrial function, leading to the disruption of $\Delta\psi_m$ in greater proportion than native etoposide (3.3% in 48 h and 4.6% in 120 h) and leading towards the apoptosis event. Apoptosis is the intrinsic death programme of a cell which plays a crucial role in the regulation of tissue homeostasis, characterized by chromatin condensation, membrane blebbing and cell fragmentation (Cohen 1993). Apoptosis is considered to be one of the mechanisms by which etoposide induces tumour regression in the retinoblastoma cell lines (Martin et al. 1995). To analyse the event, Annexin V-FITC assay was performed for the evaluation of initiation of apoptosis in cells. Annexin V is a 35- to 36-kDa phospholipid-binding protein that has high affinity to PS. In the early apoptotic event, the membrane phospholipid PS is translocated from the inner face of the plasma membrane to the cell surface and exposed to the external cellular environment to which Annexin V-FITC binds. The use of the vital dye, PI, can distinguish the apoptotic cells with intact membranes from lysed

necrotic cells. Therefore, the cells showed green staining (Annexin V-FITC) on the plasma membrane of early apoptotic cells, whereas the cells that have lost membrane integrity showed red staining (PI) throughout the nuclei and a halo of green staining (AnnexinV-FITC) on the plasma membrane. Cells that stained negative for both Annexin V-FITC and PI are alive and not undergoing measurable apoptosis. Our NP-treated cells demonstrated a significant increase of apoptotic index, ~46% (0.0005 µg/ml) and ~53.15% (0.005 µg/ml), as evident from the red fluorescence signal, whereas the native etoposide-treated cells showed early apoptotic index, ~11.56% (0.0005 µg/ml) and ~19.28% (0.005 µg/ml), as illustrated by the green fluorescence signal (Fig. 9a). Our results demonstrated that at low concentration, the nanoparticulate formulation induced more number of apoptotic and necrotic cells than that of native drug. This could be due to the higher internalization of the drug-loaded nanoparticles inside the cells, which leads to the combined effect of apoptosis and necrosis events. Since cell death is the eventual outcome of cells undergoing apoptosis, cells in the late stages of apoptosis will have a damaged membrane which stained positive for PI as well as for Annexin V-FITC.

Apoptosis was also further confirmed by DNA fragmentation, as DNA fragmentation into the oligonucleosomal ladder is the characteristic of apoptosis, and the percentage of DNA fragmentation in cultured cells exhibited a direct correlation with the percentage of apoptotic DNA (Ioannou and Chen 1996). The results demonstrated that the Y-79 cells treated with different concentrations of NPs (0.0005 and 0.005 µg/ml) underwent more DNA fragmentation as compared with native etoposide (Fig. 9b). As our formulation showed higher cytotoxic effect than native etoposide,

Fig. 8 Involvement of mitochondria in apoptosis induced by etoposide and NPs (0.0005 µg/ml) in Y-79 cells. **a** Cells incubated for 48 h. **b** Cells incubated for 120 h

a

b
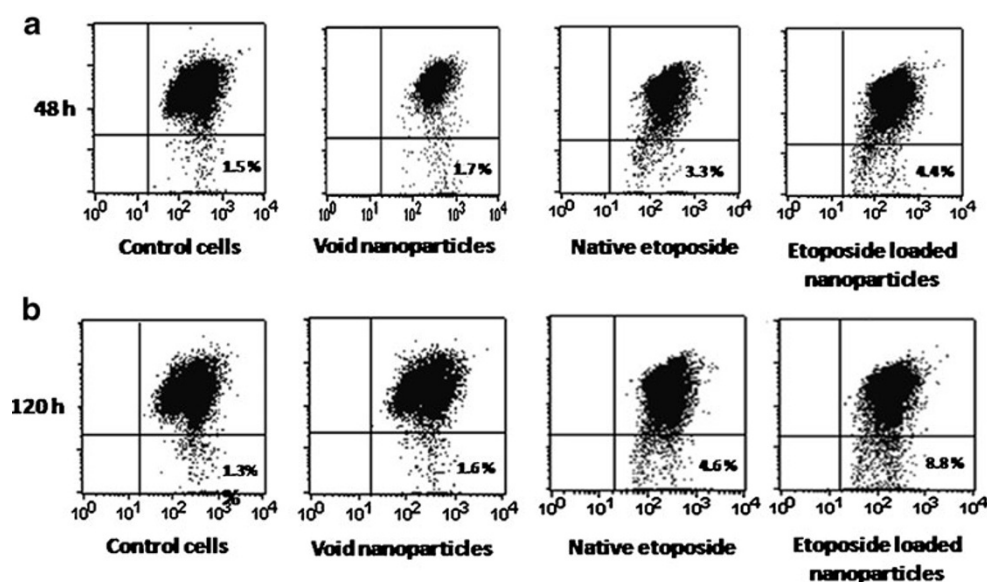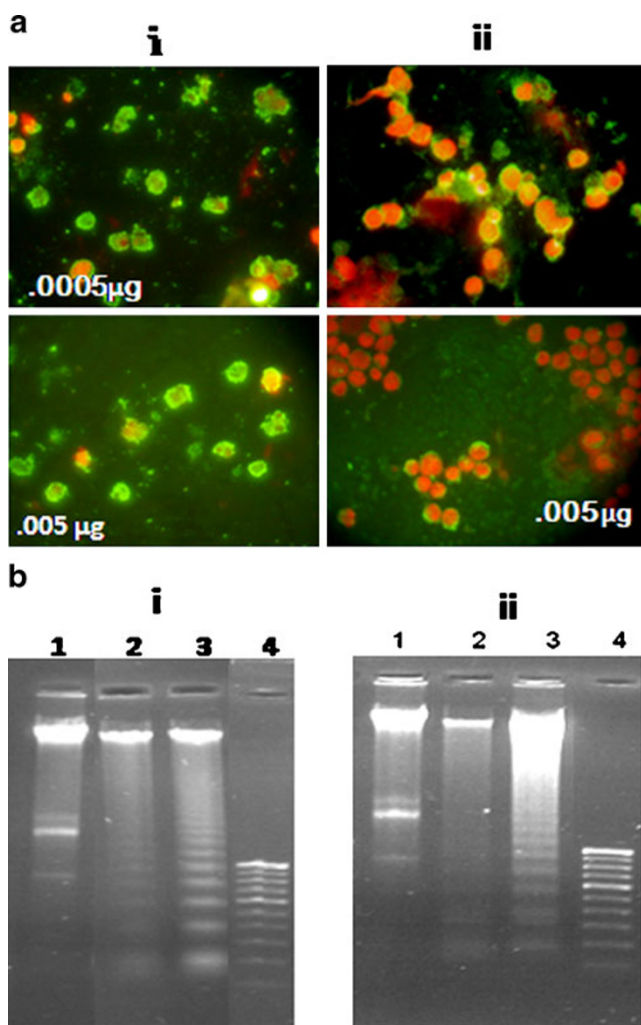
Fig. 9 a Annexin-V FITC staining for apoptosis. Y-79 cells were treated with varying concentrations of drug in solution and in nanoformulation for 5 days. The apoptotic response was determined by Annexin-V FITC and PI staining procedure. **b** Analysis of DNA fragmentation by agarose gel electrophoresis. *i* Y-79 cells treated with native etoposide and NPs (0.0005 µg/ml) for 5 days. Control cells (*lane 1*), native etoposide (*lane 2*), NPs (*lane 3*) and DNA marker (*lane 4*). *ii* Y-79 cells treated with native etoposide (0.005 µg/ml) and NPs (0.005 µg/ml) for 5 days. Control cells (*lane 1*), native etoposide (*lane 2*), NPs (*lane 3*) and DNA marker (*lane 4*)

this could be one of the reasons of showing relatively greater apoptosis in the case of cells treated with NPs.

3.9 cDNA microarray screening for potential gene expression changes induced by etoposide loaded in nanoparticles in cells

We have shown our interest to discover the potential gene expression changes in Y-79 cells after treatment with NPs mainly for two reasons. One reason is that the Y-79 cells form tumours in the murine models that closely resemble the naturally occurring tumuor in anatomic sites without

disrupting the choroids and sclera or involving the anterior chamber (Chévez-Barrios et al. 2000). The second reason is that RB tumours found in Indian RB patients are mostly advanced tumours, presenting with choroidal and optic nerve invasion (Moutushy et al. 2010). Therefore, the Y-79 cell line is appropriate for in vitro studies and the data can be translated to actual tumour state. In order to screen and compare the potential gene expressional changes occurring in the Y-79 cells treated with (0.0005 µg/ml) of NPs and with native etoposide, RNA was extracted from Y-79 cells to perform cDNA microarray analysis.

3.10 Identification of genetic networks through upregulation and downregulation of various genes

Etoposide is one of the potential drugs that are currently being used for retinoblastoma treatment. This is the first report that demonstrated the delivery of etoposide drug in nanoparticulate formulation to the retinoblastoma cells and its modulation of gene activity. Our microarray analysis revealed differential regulation of various genes which played an active role towards cell apoptosis and oncogenesis. The results of the cDNA microarray revealed the changed expression of genes (upregulation of 171 genes, downregulation of 280 genes) in the retinoblastoma cell line treated with etoposide nanoparticles and native etoposide; however, the etoposide nanoparticles illustrated an enhanced upregulated gene expression level and downregulated gene expression level, depicted in the cluster diagram (Fig. 10a and Electronic supplementary material (ESM) Tables S1 and S2). Only genes with $p \leq 0.05$ and log ratio of at least 2.0 were taken for upregulation, and a log ratio of 0.5 was considered for downregulation. In both the biologic replicates, the median log ratio of 1 was considered for expression analysis.

The microarray analysis demonstrated that NP treatment primarily upregulated the expression of three groups of potential genes related to cell cycle and cell differentiation, cell migration, apoptosis and few anti-apoptosis-related genes. Amongst them, seven genes are upregulated more than onefold in apoptosis, such as *Homo sapiens* (BCL2-antagonist of cell death (BAD), caspase 8, apoptosis-related cysteine peptidase (CASP8; Polzien et al. 2009), growth arrest and DNA damage-inducible, alpha (GADD45A), PERP, TP53 apoptosis effector (PERP), tumour necrosis factor TNF receptor-associated factor 1 (TRAF1; Kim et al. 2010), caspase recruitment domain family, member 14 (CARD14) and members of the tumour necrosis factor receptor superfamily (TNFRSF17, TNFRSF1B, TNFRSF10B, TNFRSF19; Coffer et al. 1998). Two cell cycle and cell differentiation genes, i.e. nuclear factor of kappa light polypeptide gene enhancer in B cells inhibitor, alpha (NFKBIA, platelet-derived growth factor alpha polypeptide (PDGFA), and two anti-
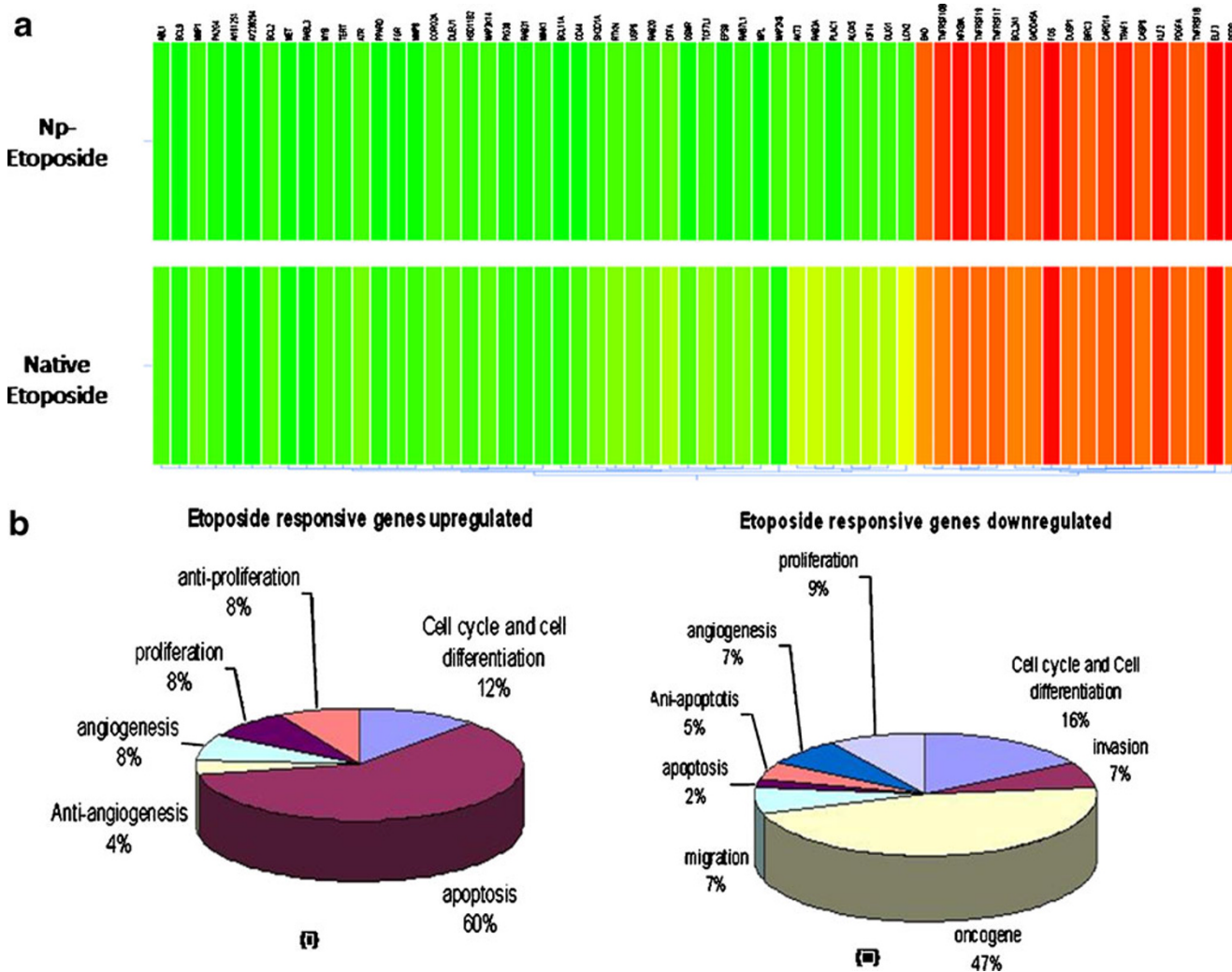
Fig. 10 **a** Display of microarray images of Y-79 cells treated with (0.0005 μg/ml) of native etoposide and (0.0005 μg/ml) NPs. *Horizontal line* represents the average expression of the individual genes modified. *Red* and *green* indicate the increased and decreased expression of genes. The figure represents one of the three replicates. **b** Functional grouping of upregulated genes (*i*) and downregulated genes (*ii*) in Y-79 cells treated with NPs. All the distinct gene identification were examined for their known biologic functions according to gene oncology convention and grouped in the respective functional category. The proportion of each functional category in the total number of selected identified genes (taken as 100%) is shown

apoptosis, i.e., baculoviral IAP repeat-containing 3 (BIRC3), transcript variant 1, BCL2-related protein A1 (BCL2A1), mRNA were upregulated. Similarly, angiogenesis factor genes, i.e. E74-like factor 3 (ets domain transcription factor, epithelial-specific; ELF3) and Kruppel-like factor 2 (lung; KLF2), were also upregulated. Moreover, one gene for cell proliferation, i.e. v-fos FBJ murine osteosarcoma viral oncogene homolog (FOS), and anti-proliferation, i.e. dual specificity phosphatase 1 (DUSP1), were upregulated too (details in ESM Tables S1 and S2). On the other hand, NP action also resulted in the significant downregulation of genes (less than onefold) related to cell cycle cell differentiation, cell invasion, various oncogenes, migrations, proliferations, angiogenesis and DNA repair, as depicted in ESM Tables S1 and S2.

3.11 Functional grouping of differentially expressed genes

All the distinct gene identifications were examined for their known biologic function according to gene ontology convention and grouped in their respective functional category. The proportion of each functional category in the total number of selected identified genes (taken as 100%) was shown in Fig. 10b. Amongst the upregulated genes, the majority of genes belonged to the apoptosis functional category (60%, *i* in Fig. 10b). Therefore, it became interesting to speculate that drug delivery through nanoparticulate formulation may promote apoptosis in Y-79 cells. However, other identified genes belonged to proliferation, anti-proliferation, angiogenesis, anti-angiogenesis

and anti-apoptotic genes. Amongst the downregulated genes, one third of the total genes belonged to the oncogenic functional category (47%) and other cell cycle and differentiation groups (16%, *ii* in Fig. 10b). However, other downregulated genes belonged to cellular invasion, anti-apoptosis, proliferation, and angiogenic genes.

In particular, genes involved in oncogenic signalling and apoptotic events were discussed below. Genes related to apoptosis such as CARD14, associated with induction of apoptosis via NFKB activation (Shammas et al. 2006); TNFRSF10B, a member of the TNF-receptor superfamily (Kim et al. 2010); p53 apoptosis effector related to PMP-22 (PERP), a transcriptional target gene of p53 tumour suppressor (Davies et al. 2009); Gadd45a, a p53 effector and stress-inducible gene, like p53 (Hildesheim et al. 2002); and BAD, a pro-apoptotic member of the Bcl-2 protein family (Polzien et al. 2009), have been significantly upregulated in cells treated with etoposide. These changes were coupled with the downregulation of important oncogenes such as KIF14, FGR, AKT3, MYB and MET. The mitotic kinesin gene KIF14 has been predicted to be one of the possible oncogenes in the 1q region which was found to overexpress by more than two orders of magnitude in RB (Corson et al. 2005). Another proto-oncogene, FGR, is expressed in elevated level in invasive breast cancer and seems to have a negative impact on disease-specific survival (Mayer and Krop 2010). AKT3 serine/threonine protein kinase that has been implicated in mediating a variety of biological responses, which include inhibition of apoptosis and stimulation of cellular growth (Coffer et al. 1998), is the predominantly active family member of AKT. The increased AKT3 gene copy number and/or loss of a negative regulatory phosphatase called PTEN leads to AKT3 activation, which reduces melanoma cell apoptosis mediated through caspase-3 to promote melanoma development (Stahl et al. 2004). MYB overexpressed in colon cancer upregulates Bcl-x$_L$ and increases tumorigenesis of colon carcinoma cells by inhibiting the apoptotic process (Biroccio et al. 2001). MET hepatocyte growth factor contributes to oncogenesis and tumour progression in several human cancers and promotes aggressive cellular invasiveness that is strongly linked to tumour metastasis (Giubellino et al. 2009). Few genes leads to tumour proliferation, such as BCL2, BCL11A; cell migration MMP8, CD44 and drug resistance ABCA1, ABCC4, ABCC1, ABCA5 were also found to be significantly downregulated in response to treatment. BCL11A defines a superfamily of C2HC zinc-finger transcription factors involved in hematopoietic malignancies (Liu et al. 2006). Bcl-2 is the prominent member of a family of proteins that are responsible for dysregulation of apoptosis and prevention of death in cancer cells (Gross et al. 1999). The ABC transporters investigated might act as drug transporters and

resistance (ABCA1, ABCA5, ABCC1 and ABCC4; Gillet et al. 2004).

Our functional study showed induced apoptotic event and reduced cell proliferation, and microarray analysis revealed a wide network of etoposide responsive genes which are involved in initiating apoptosis and reducing tumour oncogenesis. This might be due to the more uptake of etoposide into cells through endocytosis via nanoparticles. Thus, NPs can persuade more apoptosis due to the accumulation of more drug as compared to the native etoposide inside the cell.

4 Conclusions

We report for the first time that drug-loaded nanoparticles affect effectively the genetic network of cancer cells, leading to enhanced apoptosis. In the current study, we have successfully prepared etoposide-loaded nanoparticles with higher entrapment efficiency, ~86% with an optimum size range. These etoposide-loaded nanoparticles displayed greater cellular drug uptake, sustained drug retention and an enhanced anti-proliferative effect of the encapsulated anti-neoplastic agent in Y-79 cancer cells. Furthermore, microarray analysis exemplifies that these drug-loaded nanoparticles could rapidly induce cell cycle disturbance by inhibiting the expression of multiple cell cycle regulatory genes and upregulating apoptotic-related genes. Thus, at present, these drug-loaded nanoparticles could focus their therapeutic strategy towards toxicity to tumour cells, but not to healthy normal cells, in a dose-limiting manner. Hence, this nanoparticulate formulation could be a more effective promising approach for expanding tumour-targeted cancer therapy.

References

Abramson DH, Servodidio CA, Nissen M (1998) Treatment of retinoblastoma with the transscleral diode laser. Am J Ophthalmol 126:733–735

Abramson DH, Beaverson K, Sangani P, Vora RA, Lee TC, Hochberg HM, Kirszrot J, Ranjithan M (2003) Screening for retinoblastoma: presenting signs as prognosticators of patients and ocular survival. Pediatrics 112:1248–1255

Acharya SDF, Sahoo SK (2009) Targeted epidermal growth factor receptor nanoparticle bioconjugates for breast cancer therapy. Biomaterials 30:5737–5750

Amendola BE, Lamm FR, Markoe AM, Karlsson UL, Shields J, Shields CL, Augsburger J, Brady LW, Woodleigh R, Miller C (2006) Radiotherapy of retinoblastoma: a review of 63

children treated with different irradiation techniques. Cancer 66:21–26

Ashley DM, Meier L, Kerby T, Zalduondo FM, Friedman HS, Gajjar A, Kun L, Duffner PK, Smith S, Longee D (1996) Response of recurrent medulloblastoma to low-dose oral etoposide. J Clin Oncol 14:1922–1927

Biroccio A, Benassi B, D'Agnano I, D'Angelo C, Buglioni S, Mottolese M, Ricciotti A, Citro G, Cosimelli M, Ramsay RG, Calabretta B, Zupi G (2001) c-Myb and Bcl-x overexpression predicts poor prognosis in colorectal cancer: clinical and experimental findings. Am J Pathol 158:1289–1299

Calvo P, Sánchez A, Martínez J et al (1996) Polyester nanocapsules as new topical ocular delivery systems for cyclosporine A. Pharmacol Res 13:311–315

Chan HS, Gallie BL, Munier FL, Beck Popovic M (2005) Chemotherapy for retinoblastoma. Ophthalmol Clin North Am 18:55–63

Chévez-Barrios P, Hurwitz M, Louie K, Marcus K, Holcombe V, Schafer P, Aguilar-Cordova C, Hurwitz R (2000) Metastatic and nonmetastatic models of retinoblastoma. Am J Pathol 157:1405–1412

Coffer PJ, Jin J, Woodgett J (1998) Protein kinase B (c-Akt): a multifunctional mediator of phosphatidylinositol 3-kinase activation. Biochem J 335:1–13

Cohen J (1993) Apoptosis. Immunol Today 14:126–130

Corson T, Huang A, Tsao M, Gallie B (2005) KIF14 are a candidate oncogene in the 1q minimal region of genomic gain in multiple cancers. Oncogene 24:4741–4753

Davda J, Labhasetwar V (2002) Characterization of nanoparticle uptake by endothelial cells. Int J Pharm 233:51–59

Davies L, Gray D, Spiller D, White M, Damato B, Grierson I, Paraoan L (2009) P53 apoptosis mediator PERP: localization, function and caspase activation in uveal melanoma. J Cell Mol Med 13:1995–2007

Diepold R, Kreuter J, Himber J, Gurny R, Lee VH, Robinson JR, Saettone MF, Schnaudigel OE (1989) Comparison of different models for the testing of pilocarpine eyedrops using conventional eyedrops and a novel depot formulation (nanoparticles). Graefes Arch Clin Exp Ophthalmol 227:188–193

Douglas KL, Piccirillo CA, Tabrizian M (2008) Cell line-dependent internalization pathways and intracellular trafficking determine transfection efficiency of nanoparticle vectors. Eur J Pharm Biopharm 68:676–687

Enríquez de Salamanca A, Diebold Y, Calonge M, García-Vazquez C, Callejo S, Vila A, Alonso MJ (2006) Chitosan nanoparticles as a potential drug delivery system for the ocular surface: toxicity, uptake mechanism and in vivo tolerance. Invest Ophthalmol Vis Sci 47:1416–1425

Friend SH, Horowitz JM, Gerber MR, Wang XF, Bogenmann E, Li FP, Weinberg RA (1987) Deletions of a DNA sequence in retinoblastomas and mesenchymal tumors: organization of the sequence and its encoded protein. Proc Natl Acad Sci USA 84:9059–9063

Garcion E, Lamprecht A, Heurtault B, Paillard A, Aubert-Pouessel A, Denizot B, Menei P, JP B (2006) A new generation of anticancer, drug-loaded, colloidal vectors reverses multidrug resistance in glioma and reduces tumor progression in rats. Mol Cancer Ther 5:1710–1722

Gillet J, Efferth T, Steinbach D, Hamels J, de Longueville F, Bertholet V, Remacle J (2004) Microarray-based detection of multidrug resistance in human tumor cells by expression profiling of ATP-binding cassette transporter genes. Cancer Res 15:8987–8993

Giubellino A, Linehan W, Bottaro D (2009) Targeting the Met signaling pathway in renal cancer. Expert Rev Anticancer Ther 9:785–793

Gross A, Mc Donnell J, Korsmeyer S (1999) Bcl-2 family members and the mitochondria in apoptosis. Genes Dev 13:1899–1911

Hande KR (1992) Etoposide pharmacology. Semin Oncol 19:3–9

Harmia T, Speiser P, Kreuter J (1986) A solid colloidal drug delivery system for the eye: encapsulation of pilocarpin in nanoparticles. J Microencapsul 3:3–12

Hashizoe M, Ogura Y, Takanashi T, Kunou N, Honda Y, Ikada Y (1997) Biodegradable polymeric device for sustained intravitreal release of ganciclovir in rabbits. Curr Eye Res 16:633–639

Hildesheim J, Bulavin D, Anver M, Alvord W, Hollander M, Vardanian L, Fornace AJ Jr (2002) Gadd45a protects against UV irradiation-induced skin tumors, and promotes apoptosis and stress signaling via MAPK and p53. Cancer Res 64:7305–7315

Ioannou YA, Chen FW (1996) Quantitation of DNA fragmentation in apoptosis. Nucleic Acid Res 24:992–993

Jasti BR, Du J, Vasavada RC (1995) Characterization of thermal behavior of etoposide. Int J Pharmaceu 118:161–167

Kim J, Kim E, Kim S, Taeg Kyu Kwon T, KS SC (2010) Capsaicin sensitizes malignant glioma cells to TRAIL-mediated apoptosis via DR5 upregulation and survivin downregulation. Carcinogenesis 31:367–375

Lemoine D, Francois C, Kedzierewicz F, Preat V, Hoffman M, Maincent P (1996) Stability study of nanoparticles of poly(E-caprolactone), poly (D,L-lactide) and poly (D,L-lactide-co-glycolide). Biomaterials 17:2191–2197

Liu H, Ippolito GC, Wall JK, Niu T, Probst L, Lee BS, Pulford K, Banham AH, Stockwin L, Shaffer AL, Staudt LM, Das C, Dyer MJ, Tucker PW (2006) Functional studies of BCL11A: characterization of the conserved BCL11A-XL splice variant and its interaction with BCL6 in nuclear paraspeckles of germinal center B cells. Mol Cancer Ther 5:1–18

Marchal-Heussler L, Sirbat D, Hoffman M, Maincent P (1993) Poly (epsilon-caprolactone) nanocapsules in carteolol ophthalmic delivery. Pharm Res 10:386–390

Martin SJ, Reutelingsperger CP, McGahon AJ, Rader JA, van Schie RC, LaFace DM, Green DR (1995) Early redistribution of plasma membrane phosphatidylserine is a general feature of apoptosis regardless of the initiating stimulus: inhibition by overexpression of Bcl-2 and Abl. J Exp Med 182:1545–1556

Mayer E, Krop I (2010) Advances in targeting SRC in the treatment of breast cancer and other solid malignancies. Clin Cancer Res 16:3526–3532

Misra R, Sahoo SK (2010) Intracellular trafficking of nuclear localization signal conjugated nanoparticles for cancer therapy. Eur J Pharmaceu Sci 39:152–163

Misra R, Acharya S, Dilnawaz F, Sahoo SK (2009) Sustained antibacterial activity of doxycycline-loaded poly(D,L-lactide-co-glycolide) and poly(epsilon-caprolactone) nanoparticles. Nanomedicine (Lond) 4:519–530

Moutushy M, Mallikarjuna K, Verma RS, Uma M, Krishnakumar S (2010) Genome-wide changes accompanying knock-down of Ep-CAM in retinoblastoma. Mol Vis 16:828–842

Noh W, Mondesire W, Peng J, Jian W, Zhang H, Dong J (2004) Determinants of rapamycin sensitivity in breast cancer cells. Clin Cancer Res 10:1013–1023

Panyam J, Labhasetwar V (2003) Biodegradable nanoparticles for drug and gene delivery to cells and tissue. Adv Drug Deliv Rev 55:329–347

Panyam J, Labhasetwar V (2004) Sustained cytoplasmic delivery of drugs with intracellular receptors using biodegradable nanoparticles. Mol Pharm 1:77–84

Panyam J, Williams D, Dash A, Leslie-Pelecky D, Labhasetwar V (2004) Solid-state solubility influences encapsulation and release of hydrophobic drugs from PLGA/PLA nanoparticles. J Pharm Sci 93:1804–1814

Polzien L, Baljuls A, Rennefahrt U, Fischer A, Schmitz W, Zahedi R, Sickmann A, Metz R, Albert S, Benz R, Hekman M, UR R (2009) Identification of novel in vivo phosphorylation sites of the

human proapoptotic protein BAD: pore-forming activity of BAD is regulated by phosphorylation. J Biol Chem 284:28004–28020

Qaddoumi MG, Gukasyan HJ, Davda J, Labhasetwar V, Kim K-J, H-L LV (2003) Clathrin and caveolin-1 expression in primary pigmented rabbit conjunctival epithelial cells: role in PLGA nanoparticle endocytosis. Mol Vis 9:559–568

Raffaella A, Simona R, Rosanna P, Rita B, Annalisa L, Vincenzo P, Salvatore V, Maria FR (2005) Rapamycin stimulates apoptosis of childhood acute lymphoblastic leukemia cells. Blood 106:1400–1406

Reddy LH, Adhikari JS, Dwarakanath SR, Sharma RK, Murthy RR (2006) Tumoricidal effects of etoposide incorporated into solid lipid nanoparticles after intraperitoneal administration in Dalton's lymphoma bearing mice. AAPS J 8:E254–E262

Rödel C, Haas J, Groth A, Grabenbauer GG, Sauer R, Rödel F (2003) Spontaneous and radiation-induced apoptosis in colorectal carcinoma cells with different intrinsic radiosensitivities: survivin as a radio-resistance factor. Int J Radiat Oncol Biol Phys 55:1341–1347

Rodriguez-Galindo CWM, Chantada G, Fu L, Qaddoumi I, Antoneli C, Leal-Leal CST, Barnoya M, Epelman S, Pizzarello L, Kane JR, Barfield R, Merchant TE, Robinson LL, Murphree AL, Chevez-Barrios P, Dyer MA, O'Brien J, Ribeiro RC, Hungerford JHE, Haik BG, Wilimas J (2008) Retinoblastoma: one world, one vision. Pediatrics 122:e763

Sahoo SK, Labhasetwar V (2005) Enhanced antiproliferative activity of transferrin-conjugated paclitaxel-loaded nanoparticles is mediated via sustained intracellular drug retention. Mol Pharm 2:373–383

Sahoo SK, Panyam J, Prabha S, Labhasetwar V (2002) Residual polyvinyl alcohol associated with poly(D,L-lactide-co-glycolide) nanoparticles affects their physical properties and cellular uptake. J Control Release 82:105–114

Sahoo SK, Ma W, Labhasetwar V (2004) Efficacy of transferrin-conjugated paclitaxel-loaded nanoparticles in a murine model of prostate cancer. Int J Cancer 112:335–340

Sahoo SK, Dilnawaz F, Krishnakumar S (2008) Nanotechnology in ocular drug delivery. Drug Discov Today 13:144–151

Shah JC, Chen JR, Chow D (1995) Preformulation study of etoposide: II. Increased solubility and dissolution rate by solid–solid dispersion. Int J Pharm 113:103–111

Shammas M, Neri P, Koley H, Batchu R, Bertheau R, Munshi V, Prabhala R, Fulciniti M, Tai YT, Treon SP, Goyal RK, Anderson KC, Munshi NC (2006) Specific killing of multiple myeloma cells by (−)-epigallocatechin-3-gallate extracted from green tea: biologic activity and therapeutic implications. Blood 108:2804–2810

Shi YJ, Zeng K, Li GF, Zhang M, Zhu XL, Sun LD, Yang XX (2008) Effects of podophyllotoxin solid lipid nanoparticles on proliferation and apoptosis of cervical carcinoma cells. Nan Fang Yi Ke Da Xue Xue Bao 5:786–788

Shirazi FH, Bahrami G, Stewart DJ, Tomiak E, Delorme F, Neol D (2001) A rapid reversed phase high performance liquid chromatographic method for determination of etoposide (VP-16) in human plasma. J Pharm Biomed Anal 25:353–356

Smit EF, Carney DN, Harford P, Sleijfer DT, Postmus PE (1989) A phase II study of oral etoposide in elderly patients with small cell lung cancer. Thorax 44:631–633

Smith LM, Donaldson SS (1991) Incidence and management of secondary malignancies in patients with retinoblastoma and Ewing's sarcoma. Oncology (Williston Park) 5:135–141

Snehalatha MVK, Saha RN, Babbar AK, Sharma RK (2008) Etoposide loaded PLGA and PCL nanoparticles II: biodistribution and pharmacokinetics after radiolabeling with Tc-99m. Drug Deliv 15:277–287

Stahl JM, Sharma A, Cheung M et al (2004) Deregulated Akt3 activity promotes development of malignant melanoma. Cancer Res 64:7002–7010

Travis LB, Holowaty EJ, Bergfeldt K, Lynch CF, Kohler BA, Wiklund T, Curtis RE, Hall P, Andersson M, Pukkala E, Sturgeon J, Stovall M (1999) Risk of leukemia after platinum-based chemotherapy for ovarian cancer. N Engl J Med 340:351–357

Van Quill KR, Dioguardi PK, Tong CT, Gilbert JA, Aaberg TM, Jr GHE, Edelhauser HF, O'Brien JM (2005) Subconjunctival carboplatin in fibrin sealant in the treatment of transgenic murine retinoblastoma. Ophthalmology 112:1151–1158

Vandana MSS (2009) Optimization of physicochemical parameters influencing the fabrication of protein-loaded chitosan nanoparticles. Nanomedicine (Lond) 4:773–785

Wong D, Billington BM, Chignell AH (1987) Pars plana vitrectomy for retinal detachment with unseen retinal holes. Graefe Arch Clin Exp Ophthalmol 225:269–271

Yadav KSS, Krutika K (2010) Formulation optimization of etoposide loaded PLGA nanoparticles by double factorial design and their evaluation. Curr Drug Deliv 7:51–64

Yasukawaa T, Ogurac Y, Tabatad Y, Kimurae H, Wiedemanna P, Honda Y (2004) Drug delivery systems for vitreoretinal diseases. Prog Retin Eye Res 23:253–281

Zimmer A, Chetoni P, Saettone M, Zerbe H, Kreuter J (1995) Evaluation of pilocarpine-loaded albumin nanoparticles as controlled drug delivery systems for the eye. II. Co-administration with bioadhesive and viscous polymers. J Cont Rel 33:31–46